Supporting Information

Hetero-metallic Active Sites Coupled with Strong Reductive Polyoxometalate for Selectively Photocatalytic CO_2-to-CH_4 Conversion in Water

Shuai-Lei Xie[a], Jiang Liu[b]*, Long-Zhang Dong[b], Shun-Li Li[b], Ya-Qian Lan*[b], Zhong-Min Su*[ac]

[a]*Institute of Functional Material Chemistry, Department of Chemistry, National & Local United Engineering Lab for Power Battery, Northeast Normal University, Changchun 130024, P. R. China. E-mail: zmsu@nenu.edu.cn.*

[b]*School of Chemistry and Materials Science, Jiangsu Key Laboratory of Biofunctional Materials, Nanjing Normal University, Nanjing 210023, P. R. China*

[c]*School of Chemistry and Environmental Engineering, The Collaborative Innovation Center of Optical Materials and Chemistry, CUST, Changchun University of Science and Technology, Changchun 130028, P. R. China.*

Table of content

S1. Experimental section

S2. Synthesis of compounds of NENU-605, NENU-606 and NENU-607

S1. Experimental section

Materials and Instruments. All the chemicals were obtained from commercial sources and were used without further purification. Sodium Molybdat Dihydrat ($Na_2MoO_4{\cdot}2H_2O$) (99+%), Mo powder (99+%), Phosphoric acid (H_3PO_4) (85%), Phosphorous acid (H_3PO_3) (99+%), cobaltous chlorid hexahydrate ($CoCl_2{\cdot}6H_2O$) (99+%), Manganese chloride tetrahydrate ($MnCl_2{\cdot}4H_2O$) (99+%), $H_2C_2O_4$ (Oxalic acid) and ethylenediamine, N,N-Dimethylformamide (DMF), imidazole (99+%), 2-Aminoterephthalic acid (99+%) were analytical grade and supplied by the Shanghai Reagent Factory. The purity of both N_2 and CO_2 are 99.999%. Mo, Co, Mn and P were determined with a Plasma-SPEC(I) ICP atomic emission spectrometer (Jarrell-Ash 1100 + 2000). Infrared spectrum using the KBr pellet was measured on a Bruker Tensor 27 in the range of 4000-400 cm^{-1}. Thermogravimetric (TG) analysis was carried out on a Netzch STA449F3 analyser at a heating rate of 10 °C/min from ambient temperature to 700 °C under oxygen atmosphere. Elemental analysis (EA) were conducted using an Elementar vario EL III analyzer. The UV-Vis absorption spectra were acquired on a Shimadzu UV-2550 spectrophotometer in the wavelength range of 200–800 nm. The room temperature powder X-ray diffraction (PXRD) spectra were recorded in successive fashion in 2θ range of 5–50º on a Rigaku D/Max 2500/PC diffractometer at 40 kV, 100 mA at 293k with a Cu-target tube and a graphite monochromator and Bruker D8 Advance diffractometer. X-ray photoelectron spectroscopy (XPS) was used a Escalab 250Xi instrument from Thermo Scientific equipped with an Al Kα microfocused X-ray source and the C1s peak at 284.6 eV as internal standard. The irradiation experiments were conducted with a Xe lamp ($\lambda \geq 420$ nm, 300W). Electrochemical measurements were carried out using an electrochemical workstation CHI 660E. The isotope-labeled experiments were performed using $^{13}CO_2$ instead of $^{12}CO_2$, and the products were analyzed using gas chromatography-mass spectrometry (7890A and 5975C, Aglient).

Single Crystal Structure Determination. The single-crystal diffraction for **NENU-605 and NENU-606** were collected on D8 Venture PHOTON 100 CMOS diffractometer (Mo Kα, λ = 0.71073 Å) at 293K and Data of **NENU-607** was collected on Bruker AXS Apex II CCD diffractometer (Mo Kα, λ = 0.71073 Å) at 293 K respectively. All non-hydrogen atoms were refined with anisotropic displacement parameters. All structures were solved by the direct method and refined with the full-matrix least-squares technique on F^2 by the SHELX-2014[1] program package and Olex-2[2] software. All the solvent molecules which are highly disordered and not able to be modeled were treated by the SQUEEZE[3] routine in PLATON[4]. The topological analyses were performed with TOPOS[5]. The detailed structure determination parameters and crystallographic data are given in Table S2. The selected bond lengths of **NENU-605-606** are listed in Table S3-4. CCDC 1855993 (for

NENU-605), 1855994 (for **NENU-606**) and 1855992 (for **NENU-607**) contain the supplementary crystallographic data for this paper. These data can be obtained free of charge from The Cambridge Crystallographic Data Centre.

Photocatalytic CO_2 reduction test. Photocatalytic CO_2 reduction reaction was performed as follows: TEOA/H_2O (14:1 v/v, 30 mL) solution was poured into the 100 mL quartz reaction container, containing each photocatalyst (10 mg), [$Ru(bpy)_3$] $Cl_2 \cdot 6H_2O$ (0.01 mmol), and the reaction system was saturated by CO_2 for 30 min with a cap at 1 atm CO_2 partial pressure and then irradiated using Xe lamp ($\lambda \geq 420$ nm, 300W), meanwhile, the reaction system temperature was preserved at 20 ℃ by circulating cooling water systems. Gaseous product, CO, CH_4 from the reaction mixture, were measured by gas chromatography (GC-7900, CEAULIGHT, China) equipped with a flame ionization detector (FID) and a thermal conductivity (TCD).

Electrochemical measurements. All electrochemical measurements (photocurrent, the Mott–Schottky spots and EIS) were carried out at ambient environment using the electrochemical workstation (CHI 660e) in a standard three-electrode system: The carbon cloth (CC, 1 cm×1 cm) or ITO glass (1 cm×2 cm) modified with catalyst samples, carbon rod and Ag/AgCl were used as the working electrode, counter electrode and the reference electrode, respectively.

The as-synthesized crystals 2mg were grinded to powder and then dispersed in 1 mL of solvent (990μL EtOH and 10 μL 0.5%Nafion) by ultrasonication to form a homogeneous ink. Subsequently, 200 μL of the ink was covered onto the both side of ITO glass, and dried in room temperature for photocurrent or Mott–Schottky spots measurements. Similarly, 10mg crystals were dispersed in 1mL 0.5% Nafion aqueous solvent by ultrasonication to form a homogeneous ink, and 50 μL of the ink was covered onto the both side of carbon cloth for EIS test.

A Xenon light with an ultraviolet-cutoff filter (λ>=420 nm) was applied as the light source for Photocurrent, and 0.5 M Na_2SO_4 aqueous solution was used as the electrolyte. The Mott-Schottky plots were also measured over an alternating current (AC) frequency of 1,000 Hz, 1,500 Hz and 2000 Hz. These three electrodes were immersed in the 0.2 M Na_2SO_4 aqueous solution (pH = 6.6). Electrochemical impedance spectra (EIS) measurements were recorded over a frequency range of 100 kHz-0.1Hz with ac amplitude of 20 mV at 0 V, and 0.5 M $KHCO_3$ aqueous solution was used as the supporting electrolyte.

S2. Synthesis of compound of NENU-605 and NENU-606

Syntheses of NENU-605. NENU-605 tetrameric cluster was hydrothermally synthesized: An aqueous mixture of $Na_2MoO_4{\cdot}2H_2O$ (0.33g, 1.38mmol), Mo powder (0.1g, 1.04mmol), H_3PO_3 (0.1g, 1.22mmol), $MnCl_2{\cdot}4H_2O$ (0.2g, 1.00mmol), DMF (0.5mL), $H_2C_2O_4$ (0.1g, 1.11mmol), and 6mL distilled water was stirred for 30 min, then the critical pH was adjusted to approximately 3 with H_3PO_4 (85%) and KOH (1 M), and transfer it to a Teflon-lined reactor and kept temperature at 180 ^oC for 72 h. After 3 days, it was cooled down to room temperature at the rate of 10 ^oC / h, Finally, plenty of dark red octahetal crystals of NENU 605 were collected (76% yield based on Mo), washed by distilled water, and air-dried. Elemental anal. Calcd for Mo 36.02; Mn 8.57; P 8.21. Found: Mo 36.05; Mn 8.60; P 8.24%.

Syntheses of NENU-606. The preparation of **NENU-606** was similar to the method of **NENU-605**, expect that $CoCl_2{\cdot}6H_2O$ (0.12g, 0.50mmol) and $MnCl_2{\cdot}4H_2O$ (0.1g, 0.50mmol) were all added in solution at the same time, and increased the amount of $Na_2MoO_4{\cdot}2H_2O$ (0.62g, 2.57mmol), and the organic templates were replaced with Imidazole (0.1g, 1.47mmol) and 2-Aminoterephthalic acid (0.05g, 0.28mmol), increased the addition of distilled water to 8mL. Finally, red octahedral crystals were obtained (62% yield based on Mo), washed by distilled water, and air-dried. Elemental anal. Calcd for Mo 36.68; Co 2.40; Mn 6.65; P 8.49. Found: Mo 37.00; Co 2.37; Mn 6.62; P 8.46%.

Syntheses of NENU-607. An aqueous mixture of $Na_2MoO_4{\cdot}2H_2O$ (0.33g, 1.38mmol), Mo powder (0.1g, 1.04mmol), H_3PO_3 (0.1g, 1.22mmol), $MnCl_2{\cdot}4H_2O$ (0.1g, 0.50mmol), ethylenediamine (0.2 mL), $H_2C_2O_4$ (0.05g, 0.56mmol), DMF (1mL) and 6mL distilled water was stirred for 30 min, then the critical pH was adjusted to approximately 3.5 with H_3PO_4 (85%), then transfer it to a Teflon-lined reactor and kept temperature at 180 ^oC for 72 h. After 3 days, it was cooled down to room temperature at the rate of 10 ^oC / h. Eventually, red sheet crystals were obtained, washed by distilled water, and air-dried. Elemental anal. Calcd for Mo 36.37; Mn 1.74; P 7.83. Found: Mo 39.35; Mn 1.76; P 7.83%.

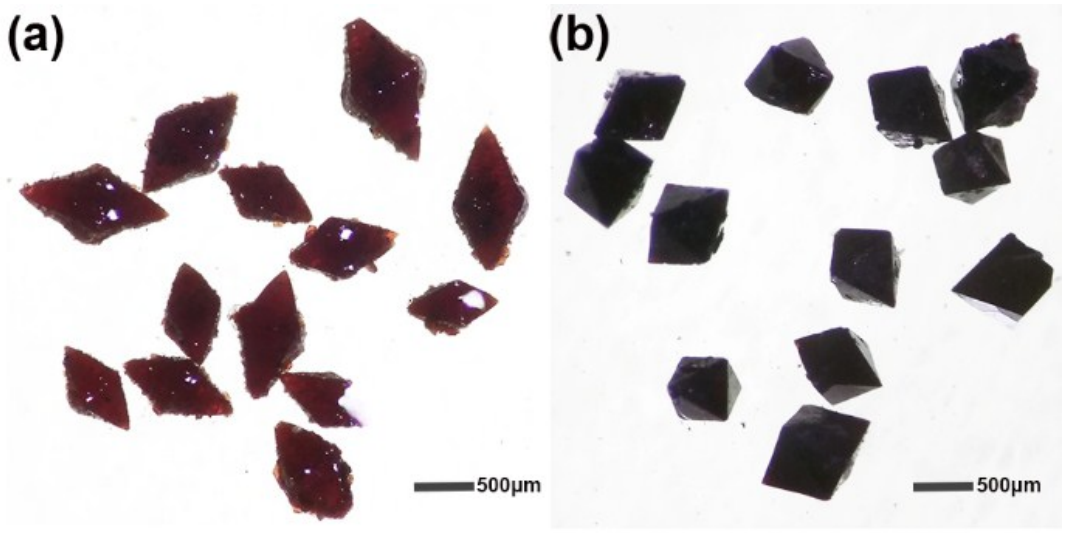

Figure S1. The photographs of **NENU-605** and **NENU-606** under an optical microscope.

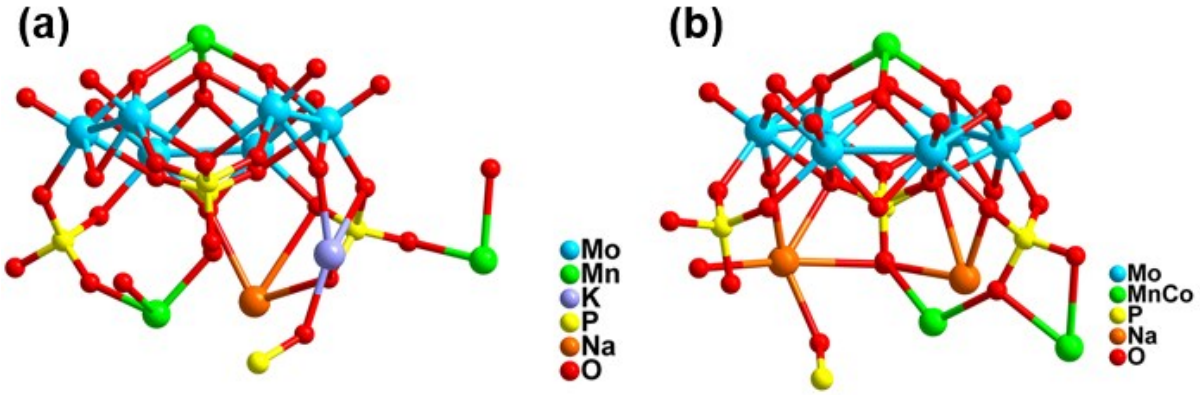

Figure S2. The asymmetric units of (a) **NENU-605** and (b) **NENU-606**.

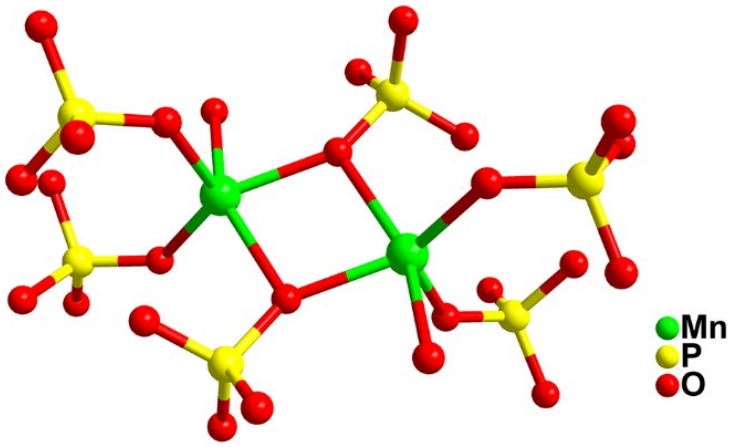

Figure S3. The coordination mode of Mn2 (**NENU-605)**, which coordinates with five O atoms from four PO_4^{3-} groups and one water molecule.

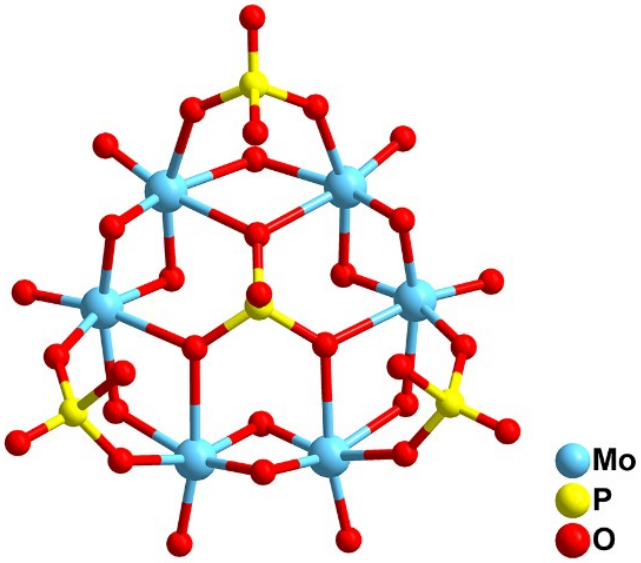

Figure S4. Ball and stick representation of $\{P_4Mo_6\}$ basic building unit.

As shown in **Figure. S4**, the most basic cell unit is $\{P_4Mo_6\}$, formed by six $\{MoO_6\}$ octahedra and four $\{PO_4\}$ tetrahedra via edge- and corner-sharing. All Mo-O and P-O bond lengths were their usual values. The central phosphate group provides three oxygen atoms that bridge the resulting hexanuclear ring, while each of the remaining three peripheral $\{PO_4\}$ groups owns two oxygen atoms to span the non-bonding Mo---Mo contacts. The four phosphate groups lie on the same side of the plane. The bond lengths of them are all within the observed range in reduced molybdenum(V) phosphates.

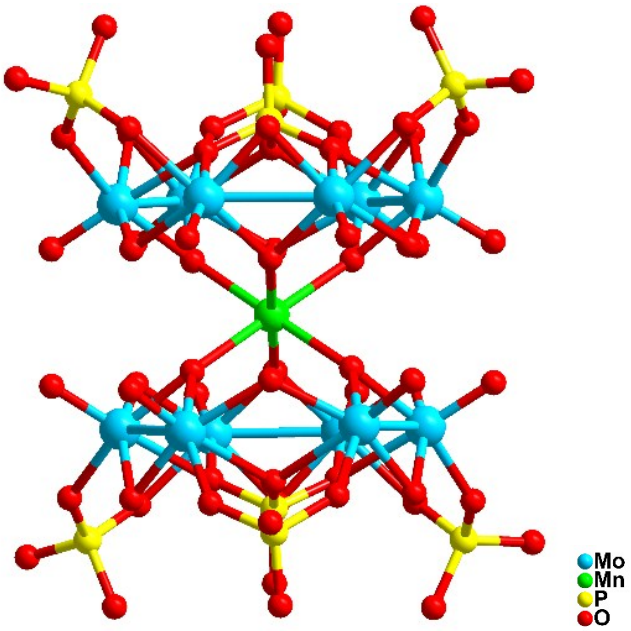

Figure S5. View of the hourglass-shaped {Mn(P_4Mo_6)} of **NENU-605**.

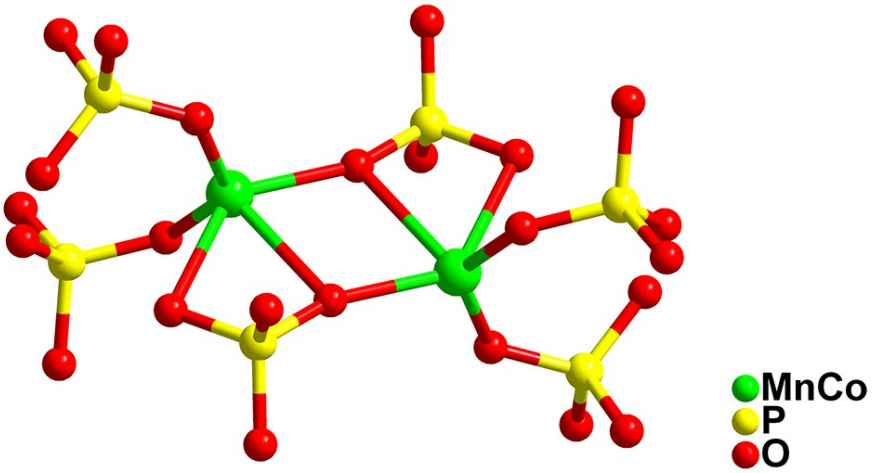

Figure S6. The coordination mode of Mn2 (**NENU-606)**, which coordinates with five O atoms from four PO_4^{3-} groups.

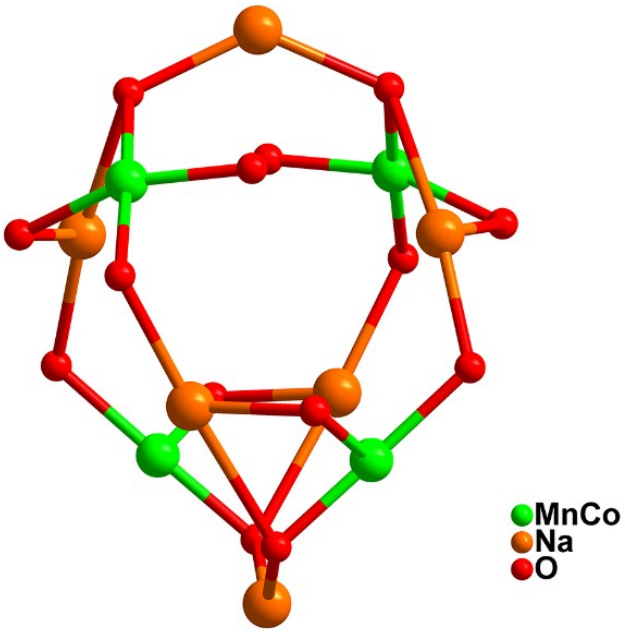

Figure S7. The shuttle-shaped second shell ({Na_6Mn_4}) of **NENU-606**, in which the locations of K1 atoms are fully replaced by Na atoms compared with **NENU-605**.

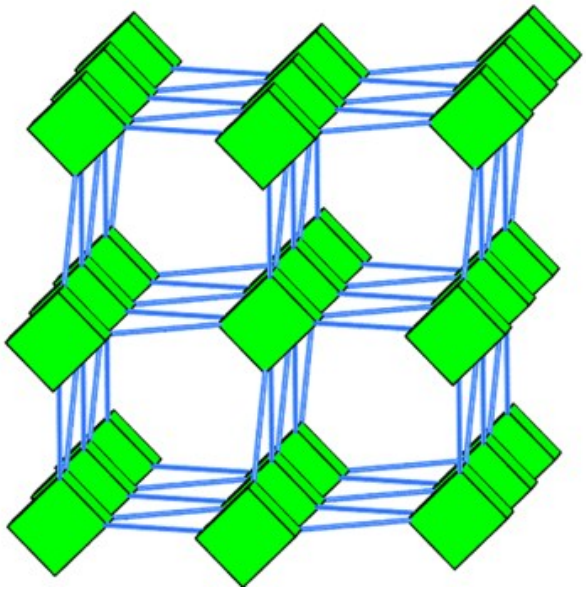

Figure S8. The topological analysis of **NENU-605** and **NENU-606**.

From the topological point of view, if the and Mn2/Mn3 atom are regarded as 8-connected nodes and linkers respectively, then the skeletons of **NENU-605** and **NENU-606** feature a unimodal topology with the Schläfli symbol of $4^{24} \cdot 6^4$. And their structures are classical body centered cubic lattice (bcu, sometimes called the CsCl net). The bcu topology is very common in metal–organic frameworks, but rare in POM-based compounds.

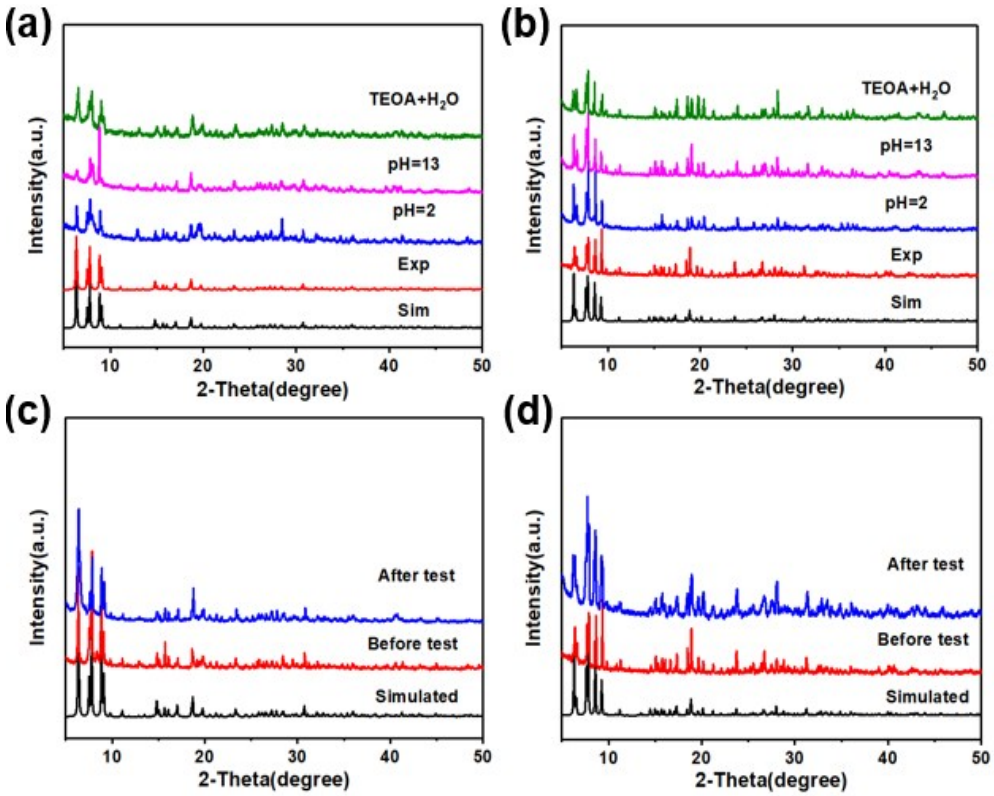

Figure S9. The PXRD patterns of (a) **NENU-605** and (b) **NENU-606** under the conditions of indicated pH values and photocatalytic reaction solution (H_2O: TEOA = 14:1 v/v, 30 mL); the PXRD patterns of (c) **NENU-605** and (d) **NENU-606** before and after photocatalytic reaction.

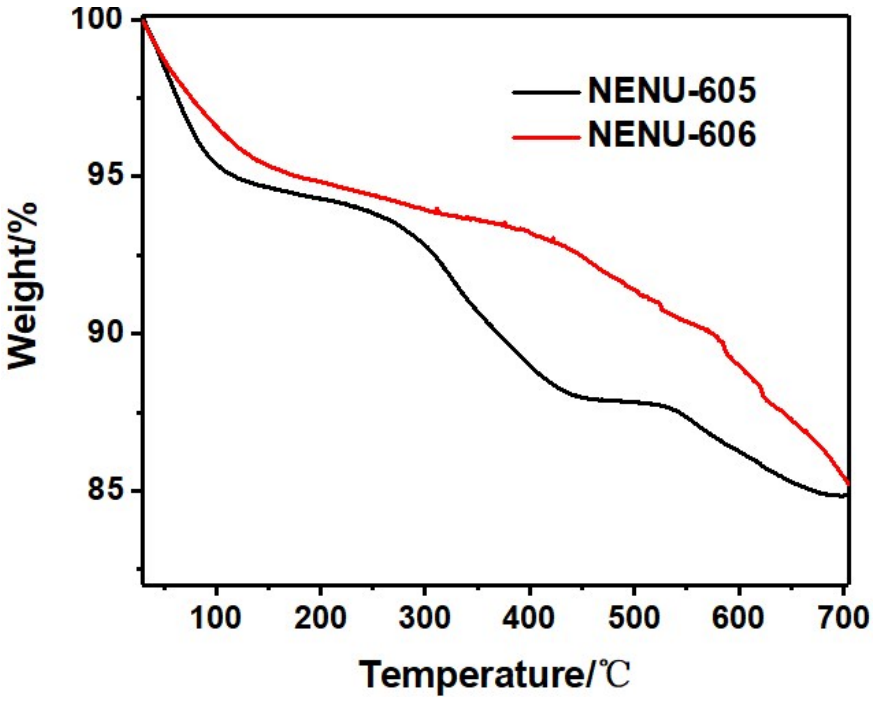

Figure S10. The TGA curve of **NENU-605** and **NENU-606** measured under O_2 atmosphere from room temperature to 700 °C at the hating rate of 10 °C · min^{-1}. A continuous weight loss of 5.95% step from 40 to 230 °C for **NENU-605** and 6.34% step from 40 to 350 °C for **NENU-606** corresponding to the loss of all lattice and coordinated water molecules.

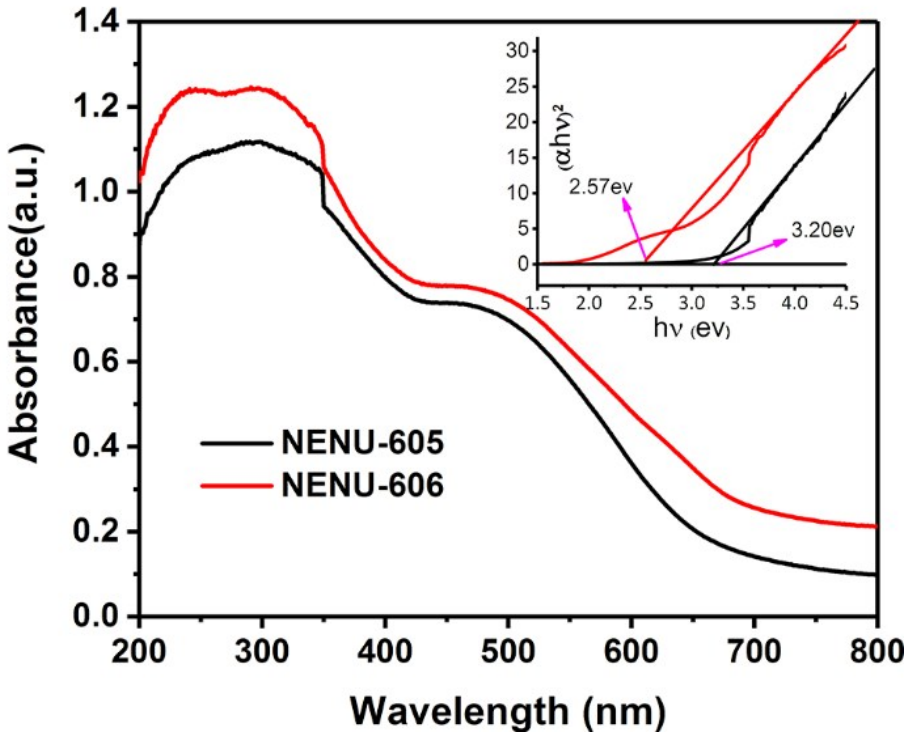

Figure S11. UV–vis diffuse reflectance spectra for **NENU-605** and **NENU-606** (inset: Diffuse reflectance UV-Vis spectrum of K–M function versus *E* (eV))

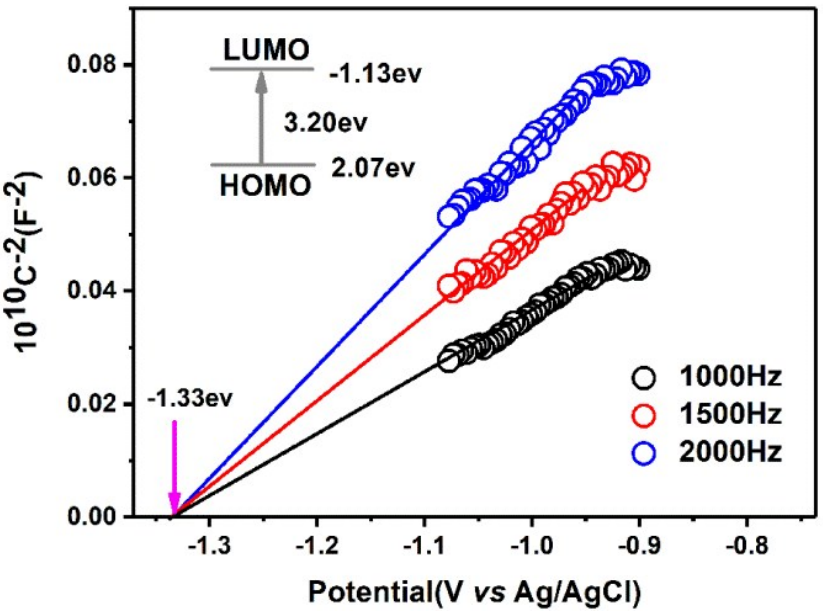

Figure S12. Mott–Schottky plot for **NENU-605** in 0.2 M Na_2SO_4 aqueous solution. Inset: Energy diagram of the HOMO and LUMO levels of **NENU-605.**

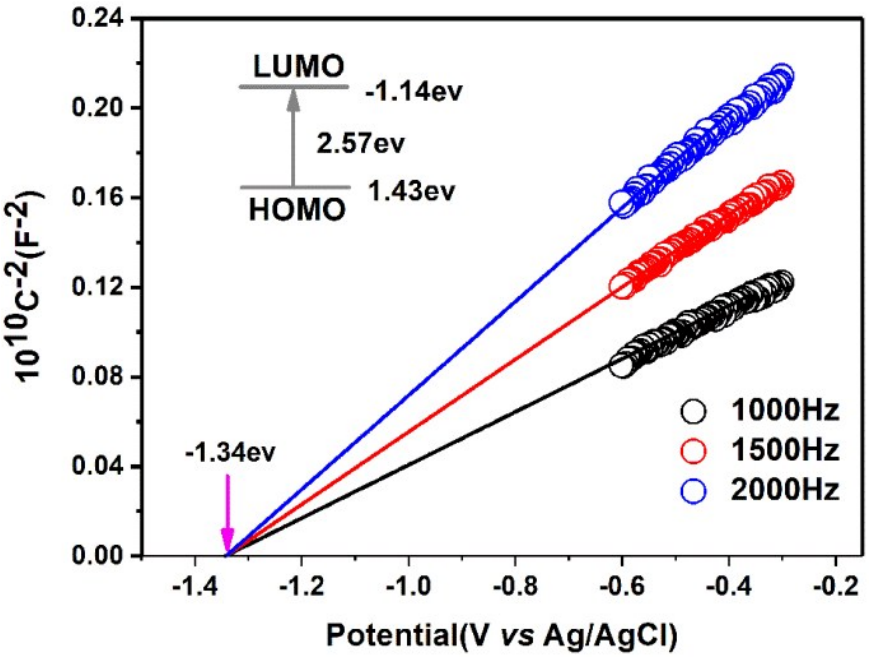

Figure S13. Mott–Schottky plot for **NENU-606** in 0.2 M Na_2SO_4 aqueous solution. Inset: Energy diagram of the HOMO and LUMO levels of **NENU-606**

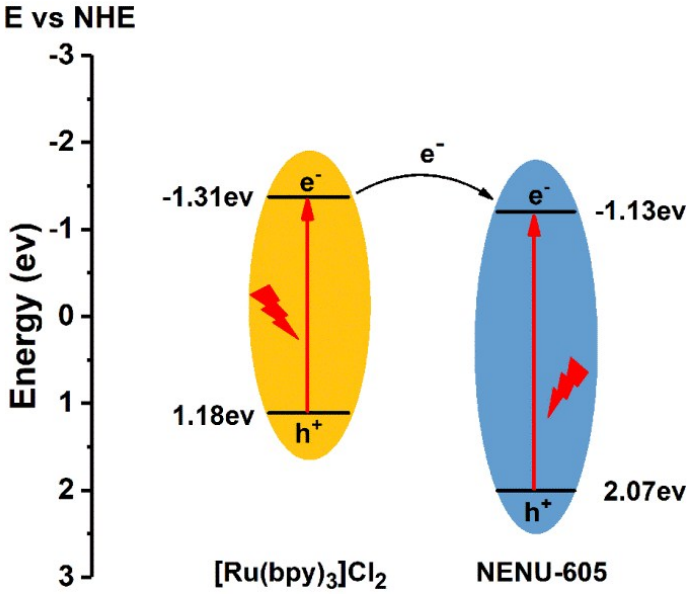

Figure S14. Schematic energy-level diagram showing electron transfer from $[Ru(bpy)_3]Cl_2$ to **NENU-605**.

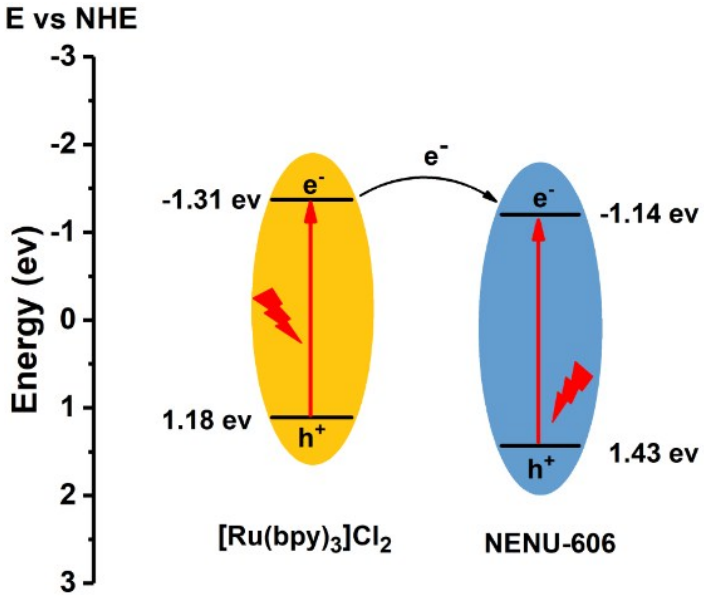

Figure S15. Schematic energy-level diagram showing electron transfer from $[Ru(bpy)_3]Cl_2$ to **NENU-606**.

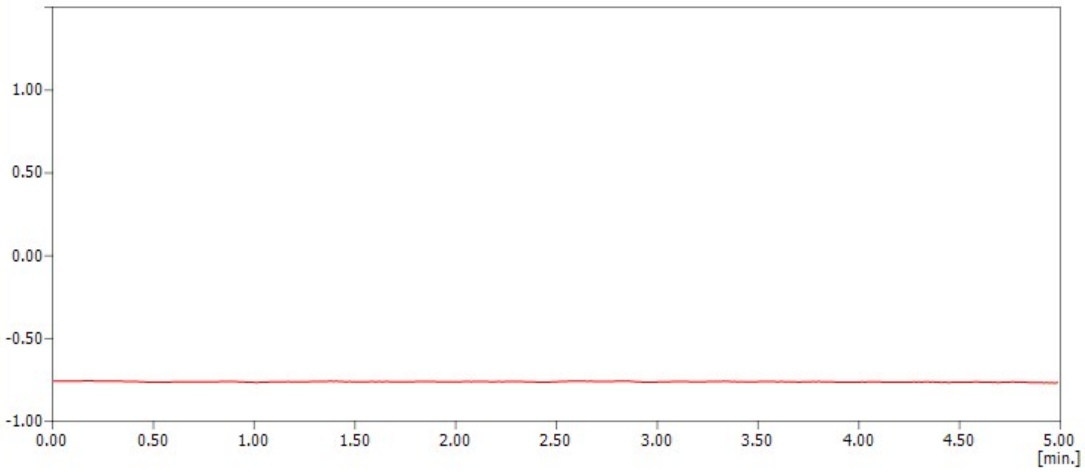

Figure S16. GC analysis of the gaseous reaction products by using the TCD.

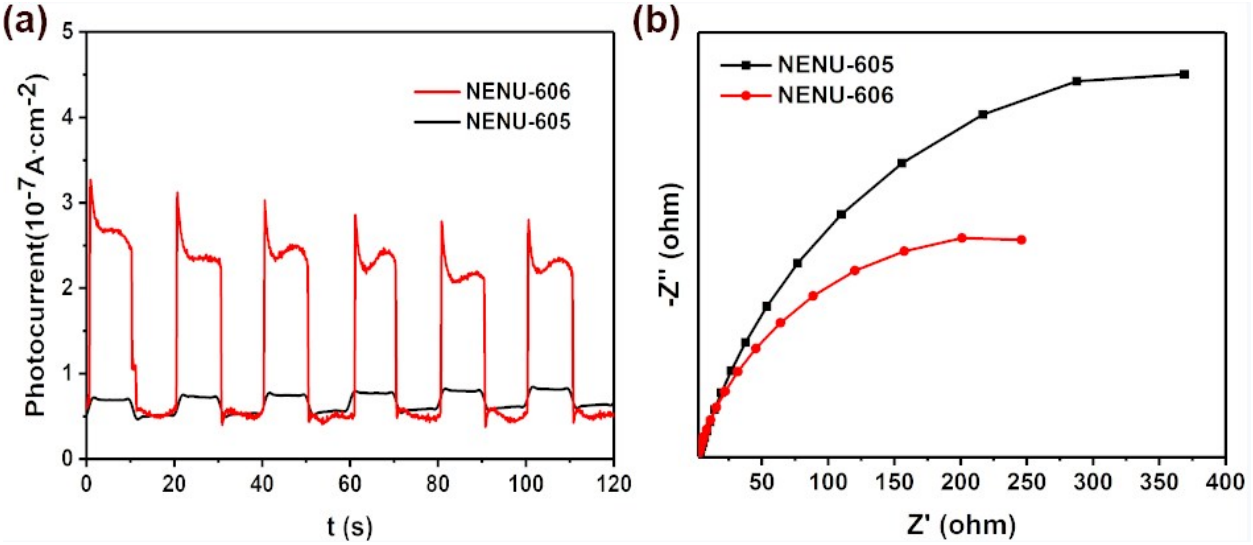

Figure S17. (a) Photocurrent responses and (b) EIS Nyquist plots.

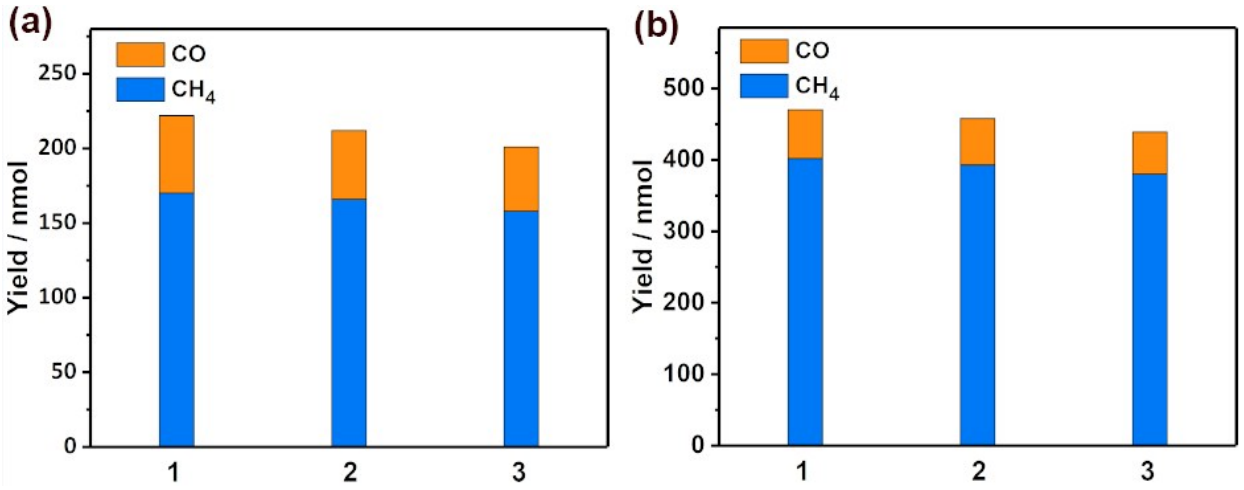

Figure S18. The recycle experiments of (a) **NENU-605** and (b) **NENU-606,** showing the durability of catalyst.

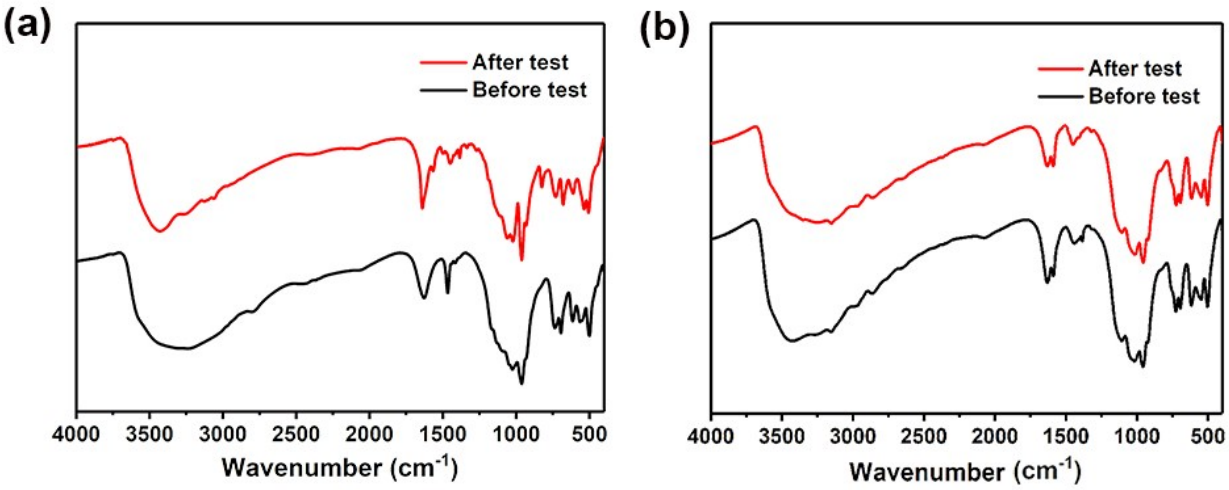

Fig S19. The IR spectra for **NENU-605** and **NENU-606** before and after reaction.

The characteristic peaks at 3440 cm^{-1}, 1622 cm^{-1} and 1456 cm^{-1} associated with the lattice, coordinated and adsorbed water molecules. The characteristic peaks of $\{P_4Mo_6\}$ at 1094, 1033, 966 and 733 cm^{-1} are attributed to *v*(P–O), *v*(Mo-O) and *v*(Mo–O–Mo) vibrations,respectively.

The IR spectra of (a) **NENU-605** and (b) **NENU-606** before and after photocatalytic test showing similar characteristics only with a slight shift indicates that they have the strong chemical stability towards photocatalytic CO_2 reduction reaction.

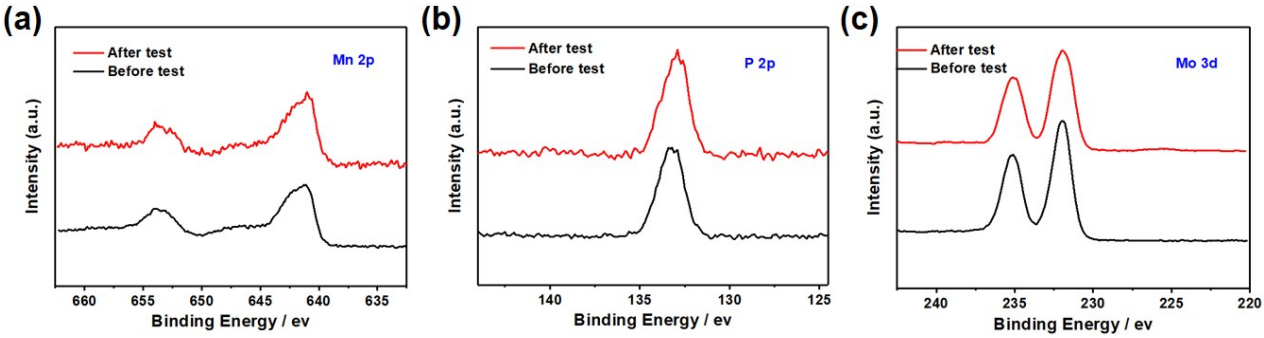

Figure S20. XPS analysis for Mn (a), P (b), Mo (c) in **NENU-605** before and after photocatalytic reduction reaction.

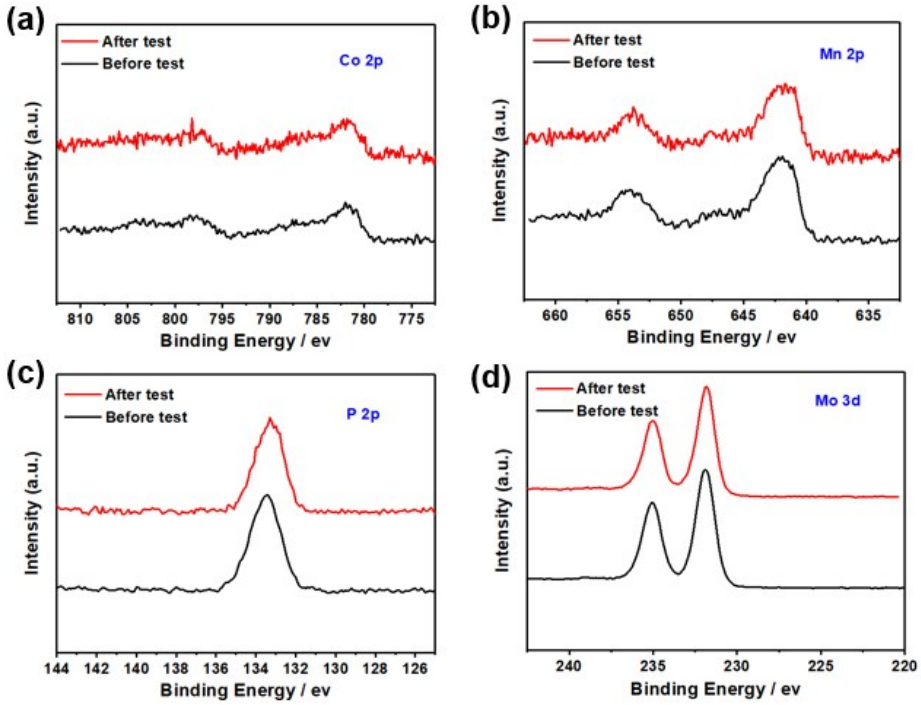

Figure S21. XPS analysis for Co (a), Mn (b), P (c), Mo (d) in **NENU-606** before and after photocatalytic reduction reaction.

As we can see from the **Figure S20 and S21**, nearly unchanged binding energies of the elements Mn 2p, Co 2p, P 2p and Mo 3d in high-resolution XPS spectra further demonstrated the structural stability of catalysts.

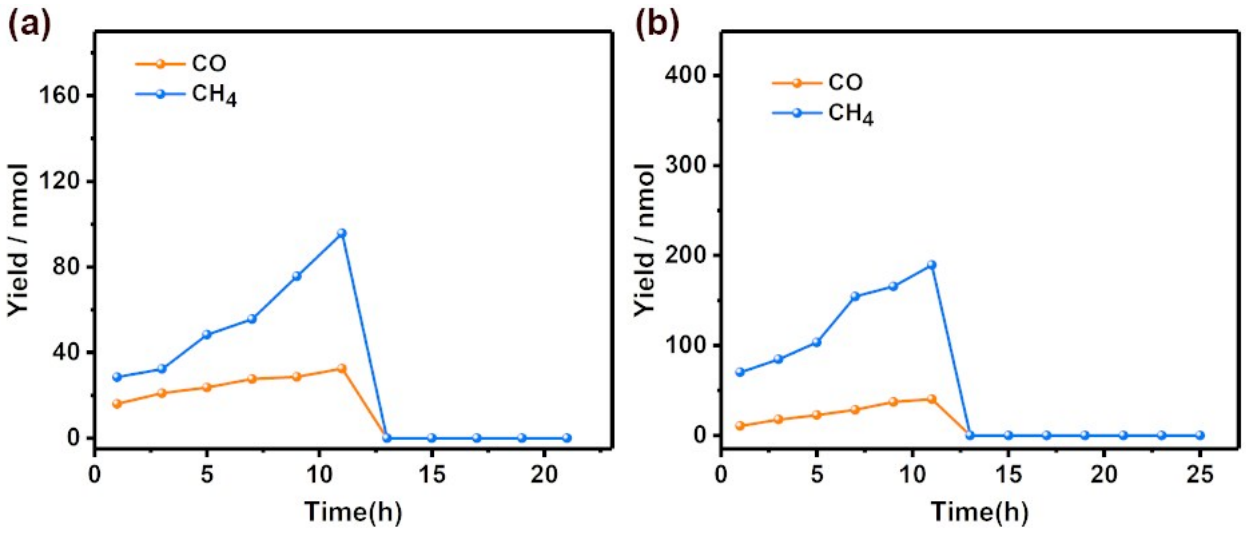

Figure S22. The additional filtrate reaction: **NENU-605** and **NENU-606** were removed from the photocatalytic system after 11 hours.

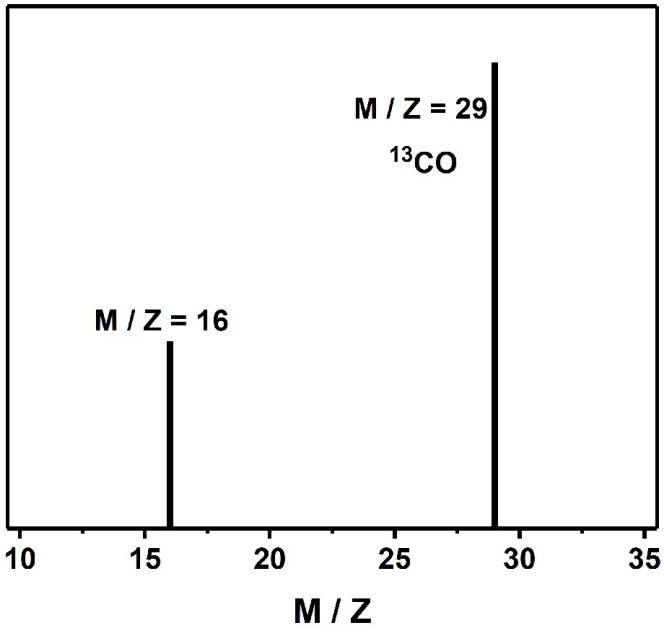

Figure S23. The Mass spectra analyses of ^{13}CO recorded under a $^{13}CO_2$ atmosphere.

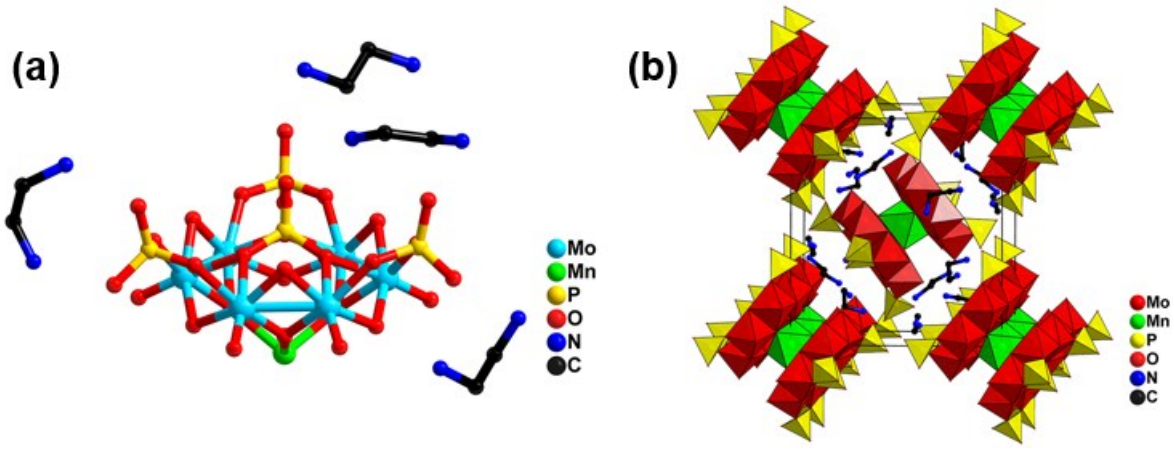

Figure S24. (a) The asymmetric unit of **NENU-607**. (b) Three–dimensional polyhedron stacking of **NENU-607**.

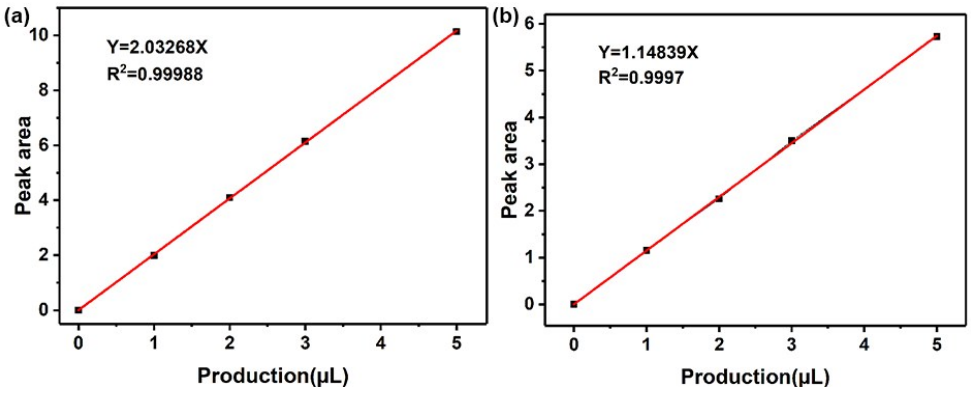

Figure S25. The standard curves of (a) CO and (b) CH_4.

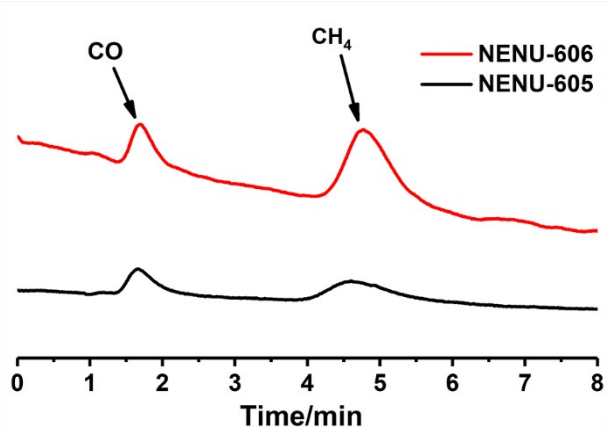

Figure S26. The GC on-line curves of **NENU-605** and **NENU-606**.

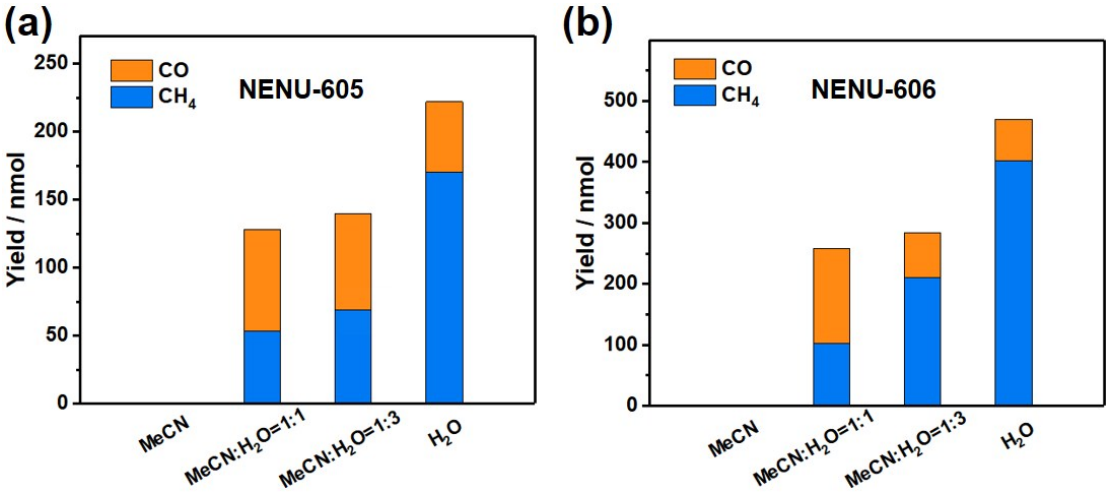

Figure S27. The influence of the reaction solvent on the photocatalytic CO_2 reduction reaction (MeCN: H_2O = 1:0, 1:1, 1:3 and 0:1)**.**

Table S1. The research of reaction conditions

entry	catalyst	conditions	CO (μmol/g)	CH_4 (μmol/g)	CH_4-TON (10^{-3})	CH_4-TOF (10^{-3} h^{-1})	All-TON (10^{-3})	All-TOF (10^{-3} h^{-1})
1	a	all	5.2	17.0	104.1	5.5	135.9	7.2
2	b	all	6.8	40.2	241.4	10.5	282.2	12.3
3	a/b	all	n.d.	n.d.			-	-
4	a/b	all	n.d.	n.d.			-	-
5	a/b	without PS	n.d.	n.d.			-	-
6	n.d.	all	n.d.	n.d.			-	-
7	a/b	without SD	n.d.	n.d.			-	-
8	d	all	4.7	7.0	15.2	0.75	25.4	1.3
9	a/b	MeCN	n.d.	n.d.			-	-

Reaction conditions: PS = $[Ru(bpy)_3]Cl_2{\cdot}6H_2O$ (0.01 mmol,), catalyst (a = **NENU-605**, b = **NENU-606 or** d = **NENU-607**) (10mg), H_2O (28 mL), SD = TEOA (2 mL), CO_2 (1 atm), λ ≥420 nm, 20℃, TON = Turnover number (mol amount of CO or/and CH_4) / (mol amount of catalyst), n.d.= Not detectable. 3 In the dark. 4 replacing CO_2 with N_2. 5 Without $[Ru(bpy)_3]$ $Cl_2{\cdot}6H_2O$. 6 Without the catalyst. 7 without sacrificial electron donor. 8 Using d = $\{P_4Mo_6\}$ basic unit instead of a or b. 9 Altering H_2O with dry MeCN.

Table S2. Crystal data and structure refinement for NENU-605, NENU-606 and NENU-607

Compound	NENU-605	NENU-606	NENU-607
Formula	$H_{308}K_{16}Mn_{40}Mo_{96}Na_8O_{616}P_{68}$	$H_{280}Co_{10}Mn_{30}Mo_{96}Na_{24}O_{602}P_{68}$	$C_{16}H_{110}MnMo_{12}N_{16}O_{74}P_8$
$D_{calc.}$/ g cm^{-3}	2.570	2.588	2.420
□/mm^{-1}	3.141	3.128	2.088
Formula Weight	25693.78	24715.70	3165.13
T/K	300.27	293.0	296.15
Crystal System	Tetragonal	Tetragonal	monoclinic
Space Group	I41/acd	I41/acd	P21/n
a/Å	27.4698(12)	26.9679(5)	15.8641(14)
b/Å	27.4698(12)	26.9679(5)	15.9370(16)
c/Å	39.881(3)	41.1540(18)	17.1695(17)
□α/°	90	90	90
□*β*/°	90	90	92.645(2)
γ/°	90	90	90
V/Å^3	30093(4)	29930.0(17)	4336.3(7)
Z	2	2	2
F(000)	21848.0	21888.0	4336.3(7)
Radiation type	MoK$_\alpha$ (λ = 0.71073)	MoK$_\alpha$ (λ = 0.71073)	MoK$_\alpha$ (λ = 0.71073)
Θ_{min}/°	2.928	2.768	1.744
□$_{max}$/°	25.703	27.502	27.721
Reflections collected	91557	83160	57163
Independent Refl.	7150	8600	10042
R_{int}	0.0619	0.0348	0.0426
GooF	1.089	1.041	1.186
wR_2 (all data)	0.1360	0.0768	0.1144
wR_2	0.1149	0.0736	0.0985
R_1 (all data)	0.0747	0.040	0.0625
R_1	0.0479	0.0316	0.0418
Largest residuals [e Å^{-3}]	1.25/-1.14	1.51/-1.15	1.28/-1.18

$^{a}R_1 = \Sigma||F_o| - |F_c||/\Sigma|F_o|$. $^{b}wR_2 = |\Sigma w(|F_o|^2 - |F_c|^2)|/\Sigma|w(F_o^2)^2|^{1/2}$.

Table S3. The selected bond Lengths in Å for NENU-605.

Atom	Atom	Length/Å
Mo1	Mo2	2.5945(11)
Mo1	O1	2.293(5)
Mo1	O5	1.964(5)
Mo1	O9	2.090(6)
Mo1	O13	1.932(6)
Mo1	O14	2.070(6)
Mo1	O22	1.675(6)
Mo2	O2	2.283(5)
Mo2	O5	1.968(6)
Mo2	O8	2.101(6)
Mo2	O12	2.053(6)
Mo2	O13	1.942(6)
Mo2	O21	1.670(6)
Mo3	Mo4	2.6075(11)
Mo3	O2	2.283(6)
Mo3	O7	1.971(6)
Mo3	O8	2.079(6)
Mo3	O11	2.049(6)
Mo3	O19	1.946(6)
Mo3	O20	1.678(6)
Mo4	O3	2.249(6)
Mo4	O7	1.984(6)
Mo4	O10	2.107(6)
Mo4	O18	2.032(7)
Mo4	O19	1.938(6)
Mo4	O25	1.673(6)
Mo5	Mo6	2.5879(10)
Mo5	O3	2.274(6)
Mo5	O6	1.975(6)
Mo5	O10	2.126(6)

Atom	Atom	Length/Å
Mo5	O16	1.946(6)
Mo5	O17	2.057(6)
Mo5	O24	1.679(6)
Mo6	O1	2.249(6)
Mo6	O6	1.966(6)
Mo6	O9	2.113(6)
Mo6	O15	2.062(6)
Mo6	O16	1.944(6)
Mo6	O23	1.673(7)
Mn1	O5	2.182(6)
Mn1	$O5^{1}$	2.182(6)
Mn1	O6	2.260(6)
Mn1	$O6^{1}$	2.260(6)
Mn1	O7	2.165(6)
Mn1	$O7^{1}$	2.165(6)
Mn2	O4	2.107(6)
Mn2	O019	2.280(8)
Mn2	O27	2.061(7)
Mn2	$O29^{3}$	2.242(7)
Mn2	$O31^{2}$	2.148(7)
Mn2	$O32^{2}$	2.189(8)
Mn3	$O26^{4}$	2.151(7)
Mn3	$O26^{2}$	2.215(7)
Mn3	$O28^{5}$	2.047(8)
Mn3	O30	2.065(7)
Mn3	O33	2.299(8)
P1	O1	1.553(6)
P1	O2	1.545(6)
P1	O3	1.551(6)
P1	O4	1.501(6)

Atom	Atom	Length/Å
P2	O14	1.555(6)
P2	O15	1.527(6)
P2	O26	1.529(6)
P2	O27	1.507(7)
P3	O11	1.550(7)
P3	O12	1.531(6)
P3	O28	1.520(8)
P3	O29	1.508(8)
P4	O17	1.534(7)
P4	O18	1.543(7)
P4	O30	1.524(7)
P4	O31	1.532(7)
P5	O32	1.515(8)
P5	O32[2]	1.515(8)
P5	O32[3]	1.515(8)
P5	O32[5]	1.515(8)

Atom	Atom	Length/Å
Na1	O16[2]	2.611(7)
Na1	O16	2.611(7)
Na1	O17[2]	2.861(7)
Na1	O17	2.861(7)
Na1	O31	2.373(8)
Na1	O31[2]	2.373(8)
O019	K1[3]	2.400(9)
O26	Mn3[6]	2.151(7)
O26	Mn3[2]	2.215(7)
O28	Mn3[3]	2.047(8)
O29	Mn2[5]	2.242(7)
O29	K1[3]	2.162(8)
O31	Mn2[2]	2.148(7)
O32	Mn2[2]	2.189(8)

[1]3/2-x, +y,1-z; [2]1-x,3/2-y, +z; [3]-1/4+y,5/4-x,3/4-z; [4]+x,1/2+y,1-z; [5]5/4-y,1/4+x,3/4-z; [6]+x, -1/2+y,1-

[1]+y,+x,+z; [2]+y,+z,+x; [3]1-z,1-x,1-y; [4]+z,+x,+y; [5]1-y,1-z,1-x; [6]1-x,1-y,1-z; [7]3/2-x,3/2-y,+z; [8]+x,3/2-y,3/2-z; [9]3/2-x,+y,3/2-z; [10]+z,+y,+x; [11]3/2-y,3/2-z,+x; [12]+z,3/2-x,3/2-y; [13]-1/2+y,1/2+x,1-z; [14]1-x,1/2+z,-1/2+y; [15]+x,+z,+y

Table S4: The selected bond Lengths in Å for NENU-606.

Atom	Atom	Length/Å
Mo1	Mo2	2.5916(5)
Mo1	O4	2.332(3)
Mo1	O7	2.085(3)
Mo1	O8	1.976(3)
Mo1	O12	1.938(3)
Mo1	O17	2.048(3)
Mo1	O22	1.674(3)
Mo2	O1	2.274(3)
Mo2	O5	2.099(3)
Mo2	O8	1.976(3)
Mo2	O12	1.937(3)
Mo2	O18	2.031(3)
Mo2	O23	1.683(3)
Mo3	Mo4	2.5916(5)
Mo3	O1	2.272(3)
Mo3	O5	2.103(3)
Mo3	O9	1.978(3)
Mo3	O13	1.943(3)
Mo3	O19	2.047(3)
Mo3	O24	1.675(3)
Mo4	O2	2.252(3)
Mo4	O6	2.115(3)
Mo4	O9	1.978(3)
Mo4	O13	1.948(3)
Mo4	O14	2.045(3)
Mo4	O25	1.680(3)
Mo5	Mo6	2.5979(5)
Mo5	O2	2.278(3)
Mo5	O6	2.098(3)
Mo5	O10	1.971(3)
Mo5	O11	1.949(3)
Mo5	O15	2.044(3)
Mo5	O20	1.680(3)
Mo6	O4	2.271(3)
Mo6	O7	2.107(3)
Mo6	O10	1.976(3)
Mo6	O11	1.941(3)
Mo6	O16	2.047(3)
Mo6	O21	1.677(3)
Mn1	O8	2.151(3)
Mn1	O8[1]	2.151(3)
Mn1	O9[1]	2.175(3)
Mn1	O9	2.175(3)
Mn1	O10[1]	2.165(3)
Mn1	O10	2.165(3)
Mn2	O3	2.146(3)
Mn2	O27[3]	2.153(4)
Mn2	O28[2]	2.092(3)
Mn2	O31	2.137(6)
Mn2	O32[2]	2.272(7)

Atom	Atom	Length/Å
Mn2	O33[3]	2.194(4)
Mn3	O26[3]	2.026(4)
Mn3	O29[2]	2.052(4)
Mn3	O30	2.425(7)
Mn3	O30[4]	2.052(5)
Mn3	O31	2.316(5)
P1	O1	1.549(3)
P1	O2	1.553(3)
P1	O3	1.502(3)
P1	O4	1.550(3)
P2	O16	1.543(3)
P2	O17	1.546(3)
P2	O26	1.511(4)
P2	O27	1.504(4)
P3	O18	1.556(3)
P3	O19	1.548(3)
P3	O28	1.511(3)
P3	O29	1.516(3)
P4	O14	1.526(3)
P4	O15	1.529(3)
P4	O30	1.489(4)
P4	O31	1.518(4)
P5	O32	1.520(7)
P5	O32[3]	1.520(7)
P5	O32[5]	1.520(7)
P5	O32[2]	1.520(7)
Na1	O13[2]	2.591(4)
Na1	O13	2.591(4)
Na1	O19	2.798(4)
Na1	O19[2]	2.798(4)
Na1	O28	2.331(4)
Na1	O28[2]	2.331(4)
Na2	O12	2.258(4)
Na2	O18	2.728(4)
Na2	O27[5]	2.252(5)
Na2	O28	2.806(5)
Na2	O32	2.236(8)
Na2	O33	2.454(5)
O26	Mn3[5]	2.026(4)
O27	Mn2[5]	2.153(4)
O27	Na2[3]	2.252(5)
O28	Mn2[2]	2.092(3)
O29	Mn3[2]	2.052(4)
O30	Mn3[4]	2.052(5)
O32	Mn2[2]	2.272(7)
O33	Mn2[5]	2.194(4)

[1]+x,1-y,1/2-z; [2]1-x,3/2-y, +z; [3]-1/4+y,5/4-x,3/4-z; [4]1/2-x,3/2-y,1/2-z; [5]5/4-y,1/4+x,3/4

Reference:

[1] D. Leggas, O. V. Tsodikov, *Acta Cryst. A* **2015**, *71*, 319-324.

[2] O. V. Dolomanov, L. J. Bourhis, R. J. Gildea, J. A. K. Howard, H. Puschmann, *J. Appl. Crystallogr.* **2009**, *42*, 339-341.

[3] A. Spek, *Acta Cryst. C* **2015**, *71*, 9-18.

[4] A. Spek, *Acta Cryst. D* **2009**, *65*, 148-155.

[5] E. V. Alexandrov, V. A. Blatov, A. V. Kochetkov, D. M. Proserpio, *CrystEngComm* **2011**, *13*, 3947-3958.